Journal of Luminescence 235 (2021) 118057

Contents lists available at ScienceDirect

Journal of Luminescence

journal homepage: http://www.elsevier.com/locate/jlumin

Disorder driven asymmetry and singular red emission in doped $Lu_2Hf_2O_7$ nanocrystals with no charge compensating defects

Santosh K. Gupta [a,b,*], Mitzy A. Penilla Garcia [c], Jose P. Zuniga [c], Bhupendra B. Srivastava [c], Yuanbing Mao [d,**]

[a] Radiochemistry Division, Bhabha Atomic Research Centre, Trombay, Mumbai, 400085, India
[b] Homi Bhabha National Institute, Anushaktinagar, Mumbai, 400094, India
[c] Department of Chemistry, University of Texas Rio Grande Valley, Edinburg, TX, 78539, USA
[d] Department of Chemistry, Illinois Institute of Technology, 3101 South Dearborn Street, Chicago, IL, 60616, USA

ARTICLE INFO

Keywords:
Disorder
Pyrochlore
Europium
$Lu_2Hf_2O_7$
Luminescence
Defect

ABSTRACT

High performance luminescent materials possess low symmetry, high color purity, no charge compensating defects, and high quantum yield. In this work, we have synthesized $Lu_2Hf_2O_7$ (LuHO) and $Lu_2Hf_2O_7$:Eu^{3+} (LuHOE) nanocrystals (NCs) using a molten salt synthesis and confirmed that both are stabilized in defect fluorite structure with a high degree of structural disordering. The LuHO NCs depicted green emission under ultraviolet irradiation, which decreases and increases after being treated in oxidizing and reducing environments, respectively, confirming the role of oxygen vacancies in the emission process. The LuHOE NCs (i) show excitation wavelength-dependent host to dopant energy transfer efficiency, (ii) give a singular red emission with high color purity of ~95%, (iii) have a dominant occupation of the Lu^{3+} sites by Eu^{3+} ions without the formation of charge compensating defects (CCDs), and (iv) possess low non-radiative channels with a quantum yield of ~88%. We believe these LuHOE NCs with singular red emission, high quantum yield, and color purity acquired through structural disordering and the absence of CCDs warrant further investigation as efficient phosphors.

1. Introduction

Phosphor-converted light emitting diodes (pc-LEDs) are revolutionizing our lighting technology owing to their high energy efficiency, robustness, low power consumption, high life span and environmentally friendliness [1–12]. The existing commercial white light phosphors exhibit high correlated color temperature (CCT) which has curtailed their favorable utilization in indoor and office lighting and marked their suitable employment for automobile lighting [13–18]. Researchers all around the globe are in continuous search for more efficient red emitting phosphors with narrow emission profile, low non-radiative channels and high quantum yield [8–12]. In this context, singular red emission (600–700 nm) with low orange interference (592 peak from $^5D_0 \rightarrow {}^7F_1$ transition in case Eu^{3+} doped phosphors) is considered ideal for pc-LEDs. It also holds great promise for bioimaging applications owing to its deep penetration, low autofluorescence, low scattering, and almost no damage to tissue [19,20]. Singular red emission has been mostly investigated in upconversion phosphors (UCPs) and very few studies have been focused on downconversion phosphors (DCPs) [19–24]. This is mainly because of the preferable NIR excitation involved in UCPs compared to UV excitation in DCPs for bioimaging. Therefore, our initial work here is intended to narrow down the hosts which facilitate singular red emission as DCPs.

For most of the existing phosphors, these desirable properties are significantly affected by intrinsic surface defects (especially for nanocrystalline phosphors), charge compensating defects (CCDs), and lattice strain [25–27]. Defects are the source of non-radiative pathways, which adversely affect the emission output and quantum yield of phosphors. Designing efficient phosphors with minimal lattice strain and no CCDs requires size and charge matching between hosts and dopants. In this particular work, we selected trivalent europium ion as a red emitting dopant owing to its high color purity, long excited state lifetime, high photostability, and the ability to act as a structural and spectroscopic probe owing to unique photophysical properties with pure magnetic dipole transition (MDT, $\Delta J = \pm 1$) and hypersensitive electric dipole transitions (HEDT, $\Delta J = \pm 2$). In this context, we have chosen $Lu_2Hf_2O_7$

* Corresponding author. Radiochemistry Division, Bhabha Atomic Research Centre, Trombay, Mumbai, 400085, India.
** Corresponding author.
E-mail addresses: santoshg@barc.gov.in (S.K. Gupta), ymao17@iit.edu (Y. Mao).

https://doi.org/10.1016/j.jlumin.2021.118057
Received 4 December 2020; Received in revised form 3 February 2021; Accepted 13 March 2021
Available online 19 March 2021

(LuHO) lattice as a luminescence host owing to its high structural and thermal stability, moderate phonon energy, ability to accommodate large concentration of dopant ions, high radiation stability, wide band gap, etc. There are three major advantages associated with the selection of LuHO. First, there is not luminescence interference or background from Lu^{3+} ion as it has full shell electronic configuration $4f^{14}$. Second, Eu^{3+} doping at Lu^{3+} site does not invoke any CCDs due to the complete matching of charge. Third, lattice strain arising out of ionic size difference is minimal due to the close size match of Lu^{3+} and Eu^{3+} ions and both belong to the lanthanide ion series. Because of its favorable and unique properties, LuHO has found applications in optical coating, scintillator, nuclear waste host, medical imaging, phosphor, etc. [28–33] Related to its application as luminescence host, there are a few reports where LuHO has been doped with Eu^{3+} and Tb^{3+} to explore the photoluminescence [29,34,35]. Specifically, Pan et al. have used solution combustion method (SCM) for synthesizing $Lu_2Hf_2O_7$/Tb which has several issue compared to our molten salt synthesis (MSS) method [29]. The SCM requires very strict control on fuel/oxidant ratio and involves the release of poisonous gases such as CO_x/NO_x, so one needs to follow stringent safety protocol during the synthesis [5]. Papan et al. just reported the quantum yield value of LuHO:Eu^{3+} (LuHOE) without any detail photophysical characterization [34]. In one of our earlier work, Pokhrel et al. mainly focused on the effect of varying A site cations of pyrochlore $A_2B_2O_7$ from $Y^{3+} \rightarrow La^{3+} \rightarrow Gd^{3+} \rightarrow Lu^{3+}$ on luminescence properties of Eu^{3+} dopants [35].

Here in this work, we carried out the molten salt synthesis of LuHO and LuHOE nanocrystals (NCs) employing $NaNO_3$–KNO_3 as the molten salt. The phase and structural analysis of the LuHO and LuHOE NCs was investigated using powder X-ray diffraction (XRD) and Raman spectroscopy. Size and morphology of the LuHO and LuHOE NCs were carried out using field emission scanning electron microscopy (FESEM). The high thermal stability of LuHO as a host was established by carrying out differential scanning caloriemetry (DSC) and themogravimetric analysis (TGA). Detailed photoluminescence analysis including excitation, emission, time resolved emission, Stark analysis, and lifetime were performed on the LuHOE NCs. We have also elucidated several photophysical properties such as radiative transition rate (A_R), non-radiative transition rate (A_{NR}), internal quantum yield (IQY), branching ratios (β), Judd-Ofelt parameters, etc.

2. Experimental

The LuHO and LuHOE NCs was synthesized by a two-step process following our previous reports [36,37]. The first step involves co-precipitation of commercially available lutetium (III) nitrate hydrate ($Lu(NO_3)_3 \bullet xH_2O$, 99.999%), hafnium dichloride oxide octahydrate ($HfCl_2O{\cdot}8H_2O$, 98%), and uranyl nitrate hexahydrate ($Eu(NO_3)_3{\cdot}6H_2O$, 99.999%) without further purification by ammonia aqueous solution to obtain a single source precursor (1-x%)$Lu(OH)_3$·x%$Eu(OH)_3$·$HfO(OH)_2{\cdot}nH_2O$. Specifically, the measured reactants for 1 mmol product were dissolved in 200 ml of distilled water (18.2 MΩ at 25°C) and titrated with 200 ml of ammonium hydroxide solution (10%, diluted from concentrated NH_4OH (aq, 28–30%) during a period of 2 h. After washing with DI water thoroughly and dried, the formed precipitate was mixed with $NaNO_3$–KNO_3 (1:1 in molar ratio) by grinding. The obtained mixture then was transferred into a crucible and heated at 650 °C to get the LuHO and LuHOE NCs. Further synthesis and instrumental characterization used in this work pertain to XRD, FESEM, Raman, and PL are well documented in our earlier work [38,39].

3. Results and discussion

3.1. Phase purity and crystalline size: XRD

The XRD patterns of the LuHO and LuHOE NCs (Fig. 1a) completely match with $Lu_2Hf_2O_7$ single phase with the Fm-3m space group of the cubic crystal system. All the (hkl) planes are in line with $Lu_2Hf_2O_7$ pyrochlore with ICDD No. 00-024-1406 having defect fluorite structure (DFS). We cannot rule out the fact that these superlattice reflections are present from the LuHO and LuHOE NCs as the lab-scale copper source-based powder X-ray diffractometer is unable to detect them owing to low intensity. Therefore, being highly sensitive to metal-oxygen vibration, Raman spectroscopy was used to probe the structure of these NCs in this work, which was shown in the next section to distinguish ideal pyrochlore $A_2B_2O_6O'$ and defect fluorite $(A/B)_2O_7$ structures. In DFS, A/B cations, oxygen and oxygen vacancies are all randomly oriented in disorderly manner. The undoped and doped samples have identical XRD patterns suggesting Eu^{3+} ion has occupied the LuHO lattice and does not lead to any new phase, impurity, or structural defect. The peaks are well defined and broadened depicting the nanocrystalline nature of the samples. The crystallite sizes calculated using the Debye-Scherer equation after subtracting the instrumental broadening are 24 and 45 nm for the LuHO and LuHOE NCs, respectively. While the crystal structure of the LuHO remained the same after the Eu^{3+} doping as the DFS, doping of the larger sized Eu^{3+} ion at the small Lu^{3+} site could result in grain growth plus possible stretching of interatomic distance in the LuHO matrix.

3.2. Structural analysis: Raman spectroscopy

Raman spectroscopy is one of the most sensitive techniques to probe metal-oxygen bond vibration, making it highly efficient for structural

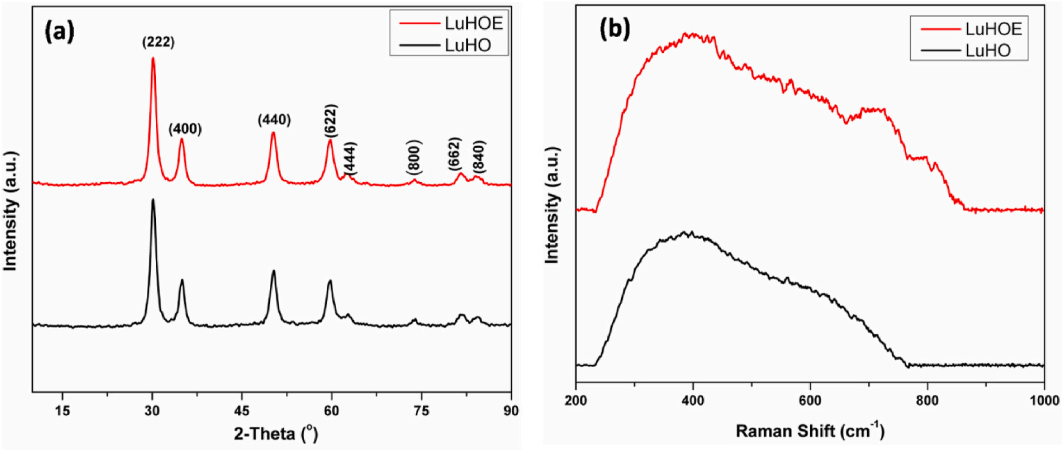

Fig. 1. (a) XRD patterns and (b) Raman spectra of the LuHO and LuHOE NCs.

analysis. Our earlier work on ordered pyrochlore structure (OPS) suggested that Raman spectrum of such phases consists of 6 peaks corresponding to $\Gamma_{OPS} = A_{1g} + E_g + 4\ F_{2g}$ [40,41]. On the other hand, DFS mainly consists of only one Raman band ascribed to $\Gamma_{DFS} = F_{2g}$. This is attributed to the fact that oxygen ion in DFS is randomly distributed over 8 anionic sites which inherently provide them with high degree of structural disordering [39,42,43]. Radius ratio of A and B cation (R_{ab}) also plays an extremely important role in dictating the structure of the same. If R_{ab} is less than 1.46, a DFS is favored, while an OPS is favorable structure when R_{ab} is greater than 1.46 [43,44]. The fact that $r(Lu^{3+}) = 0.977$ Å and $r(Hf^{4+}) = 0.83$ Å giving a $r(Lu^{3+}/Hf^{4+}) = 1.18$ also implies that LuHO will form the DFS. The Raman spectra of both LuHO and LuHOE NCs (Fig. 1b) clearly depicted one broad Raman active vibrational mode pertaining to the F_{2g} vibration ~400 cm^{-1} Eu^{3+} doping into the LuHO host does not distort its basic fluorite network which is consistent with the XRD patterns. However, the additional peaks between 700 and 800 cm^{-1} may be ascribed to the enhanced disordering of LuHO upon Eu^{3+} doping.

3.3. Morphology analysis

The FESEM images of the LuHO and LuHOE NCs (Fig. 2a and b, respectively) clearly show the formation of the LuHO NCs with particle size of ~35 nm and LuHOE NCs with size of ~50 nm. The particles are spherical in nanosized domain. Some of them are adhered to each other forming aggregates with higher degree of aggregation for the LuHOE NCs.

3.4. Optical properties

3.4.1. PL of the LuHO NCs

The emission spectrum of the air annealed LuHO NCs synthesized by the MSS method under 250 nm excitation (Fig. 3a in black) displayed a broad band peaking around 550 nm. DFS is known to possess high concentration of oxygen vacancies arranged in a random fashion. The role of oxygen vacancies in the emission process is very prominent on the basis of previous reports on PL properties of pyrochlore lattices such as $Gd_2Zr_2O_7$, $Nd_2Zr_2O_7$, $Y_2Hf_2O_7$, $La_2Zr_2O_7$, $Gd_2Hf_2O_7$, $La_2Hf_2O_7$, etc. [25,42,43,45–48] It is the combined role of neutral and ionized oxygen vacancies which have been given farfetched explanation for the appearance of visible emission from above-mentioned pyrochlore lattices. Here it is believed that the defect level of neutral and ionized oxygen vacancies lies within the band gap of LuHO NCs. Under UV excitation, the formed photoexcited holes combine with the electrons tapped inside the oxygen vacancies to give rise the broad peak at 550 nm. The color coordinate diagram of the LuHO NCs (Fig. 3b) shows bright green emission under UV irradiation.

To confirm the presence of oxygen vacancies and their role in the PL processes, the as-synthesized LuHO NCs were further annealed in either oxidizing (100% O_2) or reducing (10% H_2 + 90% Ar) atmosphere. The corresponding emission spectra are shown in Fig. 3a in black, green (oxidized) and red (reduced). It was found that the intensity of the emission band reduced and enhanced after further annealing of the as-synthesized LuHO NCs under oxidizing and reducing atmosphere, respectively. Since oxygen from the oxidizing atmosphere filled up the original oxygen vacancies substantially, and hence the emission intensity of the green band reduced after the annealing of the as-synthesized LuHO NCs under oxidizing atmosphere. On the contrary, hydrogen from the reducing atmosphere drove the formation of more oxygen vacancies, and hence the emission intensity of the green band enhanced after the annealing of the as-synthesized LuHO NCs under reducing atmosphere. The emission intensity of the green band around 550 nm followed the trend accordingly: further annealed LuHO NCs under reducing atmosphere > as-synthesized LuHO NCs > further annealed LuHO NCs under oxidizing atmosphere. Hence, this trend clearly confirms the role of oxygen vacancies in PL of the LuHO NCs.

3.4.2. PL of the LuHOE NCs

The emission spectra of the LuHOE NCs excited under several UV light wavelengths from 230 to 340 nm (Fig. 4a) demonstrated that the spectral profile does not change much in terms of Eu^{3+} emission characteristics, which suggests the charge transfer origin of all these excitation wavelengths. All these spectra exclusively show red emitting peak at 616 nm originated from the HEDT of $^5D_0 \rightarrow {}^7F_2$ which is known to appear when Eu^{3+} ion is present in highly asymmetric disordered environment. The orange peak at 593 nm (MDT, $^5D_0 \rightarrow {}^7F_1$) is extremely feeble whereas the NIR peak at 710 nm (EDT, $^5D_0 \rightarrow {}^7F_4$) is relatively weak. MDT is known to intrinsically present in emission spectra of Eu^{3+}-based luminescent materials as it is parity allowed. Its intensity further enhances when Eu^{3+} ion is located at symmetric environment with center of inversion as the local point group.

More distinguished emission spectral profile of the LuHOE NCs (Fig. 4b) was recorded upon 395 nm excitation ($^7F_0 \rightarrow {}^5L_6$), which is the one normally used in commercial applications of red phosphors. Specifically, the red emission peak is most prominent while the bands at 593 and 710 nm have much less contribution. The PL emission spectra of the LuHOE NCs displaying highly singular red emission can also be inferred from color chromaticity diagram shown in the inset of Fig. 4b with the CIE value of 0.664 and 0.312.

The color purity of the LuHOE NCs was calculated using equation (1) as reported elsewhere [11]:

$$\text{Color purity} = \frac{\sqrt{(x-x_i)^2 + (y-y)^2}}{\sqrt{(x_d-x_i)^2 + (y_d-y)^2}} \times 100\% \quad (1)$$

where (x, y), (x_d, y_d) and (x_i, y_i) are the color coordinates of the sample, dominant wavelength (616 nm in this case), and standard white illumination, respectively. In this work, (x_d, y_d) at the dominant wavelength of 616 nm was (0.681, 0.323) and the standard (x_i, y_i) coordinate is (0.310, 0.316) [12]. Accordingly, the calculated color purity of our LuHOE NCs was 95.41%, which suggest its high potential as an efficient

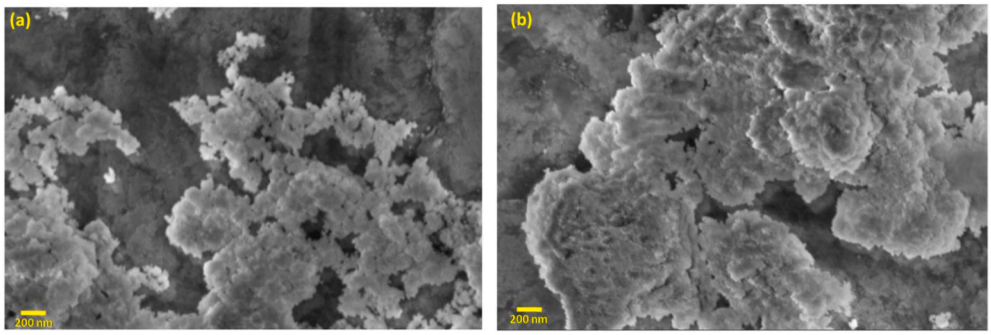

Fig. 2. FESEM images of the (a) LuHO and (b) LuHOE NCs.

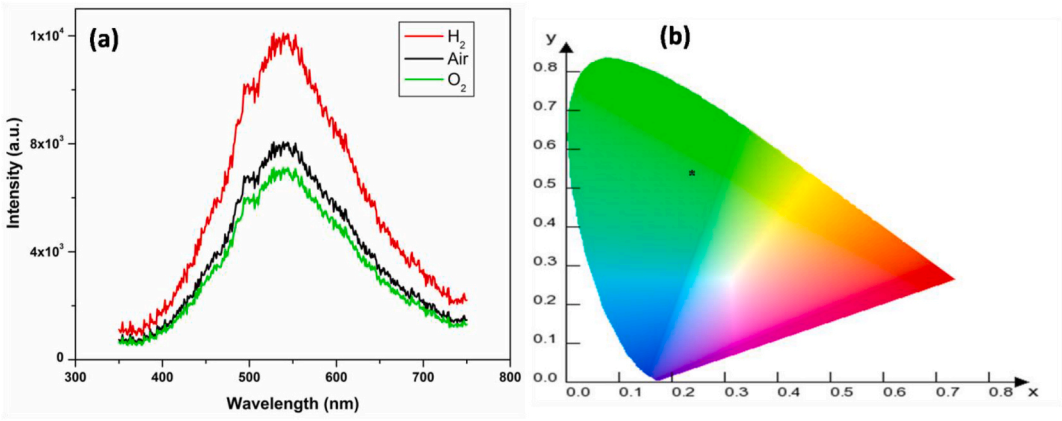

Fig. 3. PL emission spectra under 250 nm excitation of the LuHO NCs as they were originally synthesized in air and those further annealed under oxidizing and reducing atmospheres. (b) Color coordinate diagram of the LuHO NCs as originally synthesized in air.

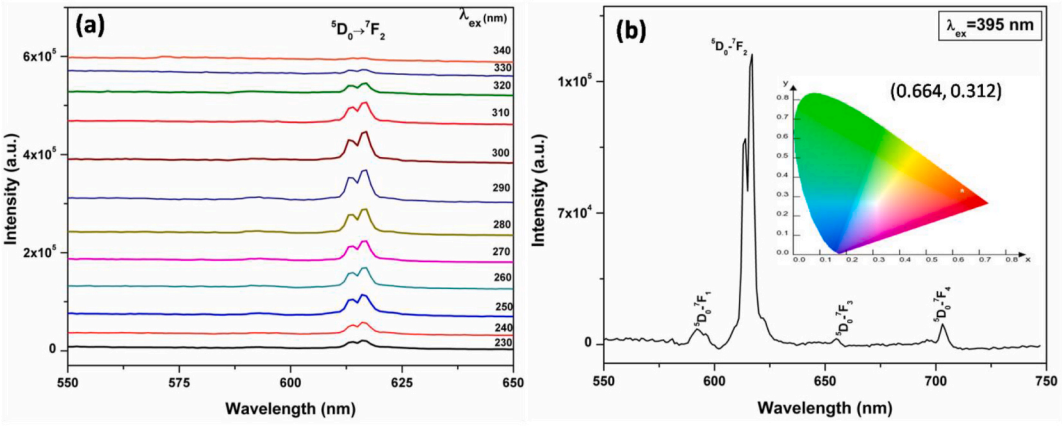

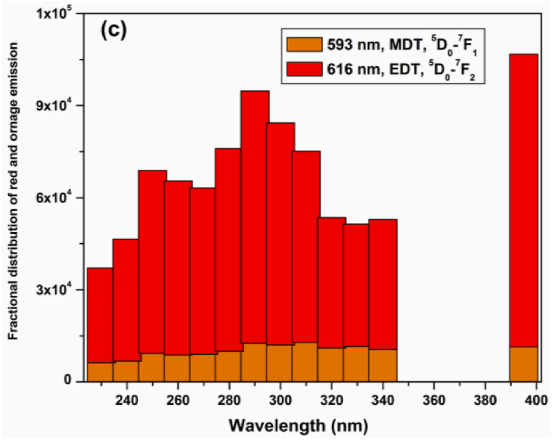

Fig. 4. PL emission spectra of the LuHOE NCs under (a) different excitation wavelengths spanning from 230 to 340 nm and (b) 395 nm excitation. Inset of Fig. 4b shows the color coordinate diagram of the LuHOE NCs at the dominant wavelength of 616 nm under 395 nm excitation. (c) Fractional distribution of red and orange emissions of the LuHOE NCs excited at different wavelengths.

red emitting phosphor for pc-LEDs.

The fractional variation of red and orange emissions of the LuHOE NCs under different excitation wavelengths was compiled in Fig. 4c. It can be clearly seen that the red emission of the HEDT peaking around 616 nm is prominently dominant while the orange contribution of the feeble MDT peak around 593 nm and the NIR contribution of the 710 nm peak are feeble in the entire spectrum. This observation suggested a singular red emission from the LuHOE NCs under different excitation wavelengths spanning across the range of 230–340 nm and at 395 nm. The fact that orange emission was not completely quenched suggests that there is more than one emission center: red emission due to hypersensitive EDT coming from Eu^{3+} at asymmetric site whereas orange emission due to pure MDT originated from Eu^{3+} at symmetric site. As discussed earlier, because of its intrinsic R_{ab} around 1.18, LuHO tends to

stabilize in DFS, which is highly disordered in nature. The local polyhedra of Lu^{3+} are in ideal cube configuration and Hf^{4+} polyhedron is in distorted octahedral configuration. Eu^{3+} doping ions energetically tend to substitute Lu^{3+} sites due to charge matching and close match of ionic radius between Eu^{3+} and Lu^{3+} ions. Even though the local symmetry around Eu^{3+} ion at Lu^{3+} cubic polyhedral is high, the overall symmetry decreases due to the intrinsic DFS, which has randomly oriented cations, anions and vacancies in disordered manner. As a result, Eu^{3+} ion is situated in highly asymmetric and distorted global environment with complete absence of center of inversion. Moreover, other spectral transitions such as $^5D_0 \rightarrow {}^7F_0$ and $^5D_0 \rightarrow {}^7F_3$, which are neither allowed by MDT nor by EDT, are not present in the PL spectra at all. Therefore, such extraordinary spectral profile leading to singular red emission is attributed to disordered DFS structure of the LuHO host couple with enhanced lattice distortion in nanocrystallites.

The PL excitation spectrum of the LuHOE NCs by monitoring emission at 616 nm corresponding to the HEDT $^5D_0 \rightarrow {}^7F_2$ of Eu^{3+} ion (Fig. 5a) consists of a broad band spanning of 225–325 nm with several embedded fine features. The broad band can be attributed to $O^{2-} \rightarrow Eu^{3+}$ charge transfer band, $O^{2-} \rightarrow Hf^{4+}$ host absorption band, and $Hf^{4+} \rightarrow Eu^{3+}$ inter-valance charge transfer band [49–51]. The intra-configurational f-f peaks observed at 364 and 395 nm can be ascribed to $^7F_{0,1} \rightarrow {}^5D_4$ and $^7F_0 \rightarrow {}^5L_6$ transitions of Eu^{3+}, respectively. Owing to forbidden nature of f → f transitions, these peaks are relatively weak in intensity compared to the charge transfer band.

The lifetime decay profile of the LuHOE NCs (Fig. 5b) shows bi-exponential decay behavior with fitting equation is as follow:

$$I = I_0 + A\ \exp(-t/\tau_1) + B\ \exp(-t/\tau_2) \quad (2)$$

where A and B are the intensities at different time intervals and τ_1 and τ_2 are their corresponding lifetimes and I_0 is the background or detector zero offset. Faster decaying component (τ_1, 364 μs, 17%) may be related to Eu^{3+} ions which are near the defects or surfaces of the LuHOE NCs, whereas the slow decay process (τ_2, 2.34 ms, 83%) is related to the Eu^{3+} localized at Lu^{3+} center [52]. And average fluorescence lifetime would be 1.79 ms. We clearly rule out any Eu^{3+} ion occupying Hf^{4+} site as have been observed in ideal pyrochlore lattices because Eu^{3+} ion occupying Hf^{4+} site is expected to offer lifetime in the range of few milliseconds [13,45,48]. As the high feasibility of Eu^{3+} ion occupying Lu^{3+} site based on the ionic radius and charge matching, Eu^{3+} ion only occupies Lu^{3+} site in the LuHOE NCs with a fraction being on the surface of the NCs as suggested by the lifetime spectra, so there is no CCDs present in the LuHOE NCs at all.

Host to dopant energy transfer is another most important and critical photophysical parameters which is quite useful in designing tunable phosphors. The energy transfer efficiency (ETE) is known to depend on excitation photon energy [53,54]. In this study, the combined emission spectra of the LuHO NCs as the host and the Eu^{3+} dopant ion in the LuHO NCs at different excitation wavelengths (Fig. 6) clearly show that: (i) the ETE increases with increasing excitation wavelength peaking around 290 nm and then it reduces with further increasing excitation wavelength; and (ii) the host emission predominates at longer wavelength zone of 300–340 nm within the employed excitation wavelength range of 230–340 nm.

4. Radiative properties of the LuHOE NCs

We have also determined the Judd-Ofelt parameters of the LuHOE NCs after excited at 395 nm to provide information related to PL quantum yield (PLQY), branching ratios, non-radiative transition probability, bond covalency and polarizability, which are extremely important in designing phosphor-converted white light emitting diodes [55]. Based on several mathematical equations described elsewhere [46,55,56], the above mentioned parameters were determined (Table 1). The most intriguing thing which can be inferred from the parameters listed in this table is the extremely low value of the non-radiative transition rate (A_{NR}). It is around 63.4 s^{-1} even though the LuHOE NCs are nanostructured and expected to have decent amount of surface defects. The extremely low value of A_{NR} is attributed to the absence of any CCDs which normally arise in case of aliovalent substitution of dopant ions in host lattices. Herein, in our LuHOE NCs, Eu^{3+} doping ion selectively occupies Lu^{3+} site, which has been inferred based on Raman, PL and lifetime spectroscopy data. As a result, there is no appearance of invoked CCDs. Radiative transition rate was found to be around 469 cm^{-1}, which is not abnormally high and is expected in the similar range in case of nanostructured phosphors. In the end, the low value of A_{NR} leads to extremely high value of internal QY (IQY) around ~88.1%, which suggests that the LuHOE NCs have high potential to be exploited as red phosphors for designing pc-LEDs. This value surpasses the IQY reported for Eu^{3+} doped ideal pyrochlore lattices.

Specifically, the IQY of the $^5D_0$ level under 395 nm excitation was calculated using equation (3):

$$IQY = \frac{A_R}{A_R + A_{NR}} \quad (3)$$

We would like to stress that this is the IQY of phosphor materials and the exact value may be lower compared to absolute value calculated using integrating sphere or low temperature measurements.

The PL decay time or the fluorescence lifetime (τ_f) of any phosphor system usually reveal the total lifetime of a particular state. That is the time taken for the particular state population to be $1/e$ of the initial value. This decay time, which can be represented as the inverse of

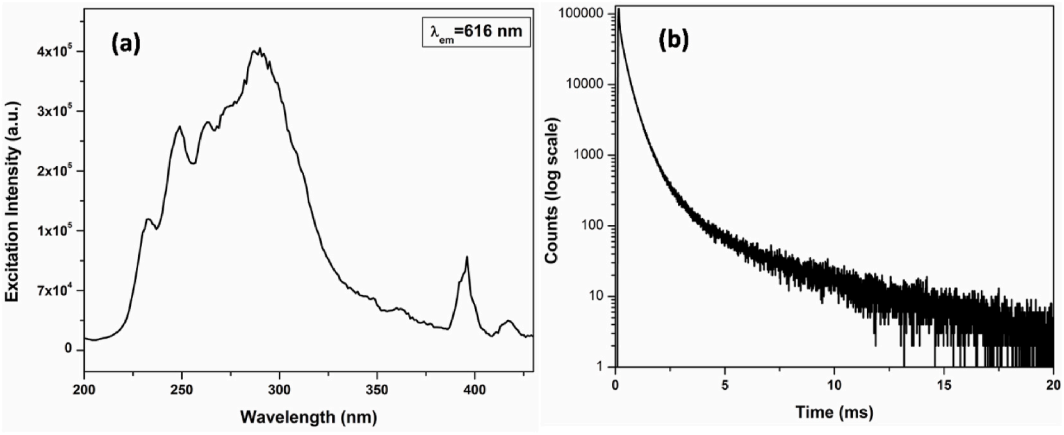

Fig. 5. (a) PL excitation spectrum of the LuHOE NCs with 616 nm emission and (b) luminescence decay profile of the LuHOE NCs under 395 nm excitation and 616 nm emission.

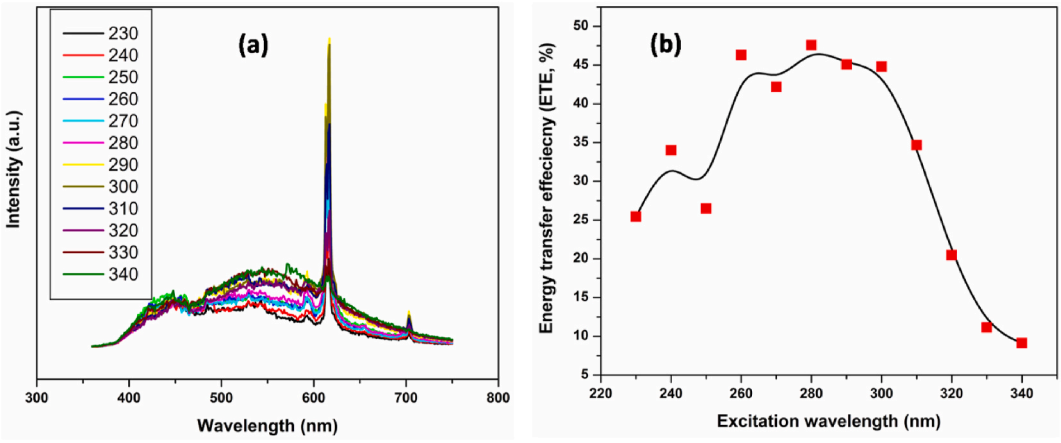

Fig. 6. (a) PL emission spectra of the LuHO host + Eu^{3+} doping ion and (b) variation of ETE with excitation wavelength of the LuHOE NCs.

Table 1
Calculated J-O parameters and radiative properties of the LuHOE NCs (A_R = radiative Rate, A_{NR} = nonradiative rate, Ω_n = the Judd−Ofelt parameter, and β_n = branching ratio).

A_R (s^{-1})	A_{NR} (s^{-1})	*IQY* (%)	Ω_2 ($*10^{-20}$)	Ω_4 ($*10^{-20}$)	β_1 (%)	β_2 (%)	β_4 (%)
469	63.4	88.1	4.57	1.28	8.1	85.7	7.2

transition rate from the upper excited state to the ground state consists of two parts that can be represented as follows.

$$\frac{1}{\tau_f} = \frac{1}{\tau_R} + \frac{1}{\tau_{NR}} \quad (4)$$

here τ_R is known as the radiative lifetime and τ_{NR} is the non-radiative lifetime. However, it is possible to determine both radiative and non-radiative lifetimes theoretically using the Judd-Ofelt (J-O) calculations by taking the inverse of A_R *and* A_{NR}. τ_R in this case would be 2.13 ms and τ_{NR} would be 15.7 ms. The PLQY calculated based on τ_f and τ_R would be 84.03%. This value is different slightly from the one (~88.1%) calculated based on the radiative and non-radiative transition rates probably because excited state lifetime is affected more by non-radiative channels.

The short-range Judd-Ofelt parameter Ω_2 gives information about covalency, symmetry and structural distortion in the surrounding of Eu^{3+} ions in the LuHOE NCs whereas the long-range Judd-Ofelt parameter Ω_4 provides bulk information, i.e. the viscosity and rigidity of host lattices [57]. This observation wherein the short-range Judd-Ofelt parameter Ω_2 is much higher than the long-range Judd-Ofelt parameter Ω_4 suggested that Eu^{3+} ions, i.e. $\Omega_2 \gg \Omega_4$ were localized in extremely disordered structure. It is consistent with the Raman spectroscopic data, which have already confirmed that the LuHOE NCs are stabilized in the highly disordered DFS. Moreover, the value of J-O ratio (Ω_2/Ω_4) is as high as 3.57, which suggests a high asymmetry of Eu^{3+} local environment in the LuHOE NCs. The fractional distribution of branching ratios suggests that a high contribution of $^5D_0 \rightarrow {}^7F_2$ transition to the PL emission of the LuHOE NCs compared to that of the orange band at 593 and the NIR band at 710 nm. These results along with the measured high PLQY suggest the high color purity of red emission from the LuHOE NCs.

Moreover, the reported values of some of the Eu^{3+}-doped pyrochlore phosphors listed in Table 2 provide a positive implication of this particular work. Owing to the absence of CCDs and low non-radiative channels in our LuHOE NCs, they outperform most of the reported Eu^{3+}-doped pyrochlore phosphors.

Table 2
Calculated J-O parameters and radiative properties of other europium doped pyrochlore nanophosphors.

Nanophosphors	A_{NR} (s^{-1})	*IQY* (%)	β_2 (%)
$Nd_2Zr_2O_7:Eu^{3+}$ [58]	63	89	–
$NaYSnMoO_7$: Eu^{3+} [59]	271	84	
$Y_2Hf_2O_7:Eu^{3+}$ [34]	205	68	
$Lu_2Ti_2O_7:Eu^{3+}$ [60]	529	61	–
$Gd_2Zr_2O_7:Eu^{3+}$ [47]	258	51	58
$La_2Zr_2O_7:Eu^{3+}$ [46]	237	62	68
$La_2Hf_2O_7:Eu^{3+}$ [61]	151	65	62
$Gd_2Hf_2O_7:Eu^{3+}$ [39]	188	64	61
$Lu_2Sn_2O_7:Eu^{3+}$ [38]	234	64	64
$Lu_2Hf_2O_7:Eu^3$ [This work]	63	88	85.7

5. Conclusions

In this work, LuHO and LuHOE NCs were developed using a molten salt synthesis method with $NaNO_3$–KNO_3 at 650 °C. XRD patterns confirmed the formation of pure disordered fluorite phase. FESEM images showed the formation of spherical nanoparticles with some of them adhered to each other to form aggregates. Raman spectroscopy suggested that both the LuHO and LuHOE NCs stabilize in defect fluorite structure with random orientations of cations, anions, and vacancies. TGA and DSC data demonstrated the exceptional thermal and chemical stability of the LuHO NCs, making them an extremely desirable luminescence host. The LuHO NCs depicted bright green emission under UV irradiation due to the recombination of photoexcited holes and electrons trapped in oxygen vacancies. The presence of oxygen vacancies and their role in the PL of the LuHO NCs were confirmed by the reduction enhancement of the green band intensity of the LuHO NCs after further annealing in an oxidizing and reducing atmosphere, respectively. Host to dopant energy transfer of the LuHOE NCs was found to be excitation energy dependent: energy transfer efficiency increased initially peaking at 290 nm and reduced thereafter, which could offer an opportunity to design color tunable phosphors by excitation wavelength. Interestingly, the PL of the LuHOE NCs showed quite strong singular red emission with weak orange and NIR contributions, which suggested that the global environment of Eu^{3+} doping ion was highly disordered in defect fluorite structure combined with their intrinsic nanostructure and crystallinity. Based on singular emission profile and lifetime spectroscopy, it was proposed that Eu^{3+} ion occupied Lu^{3+} site in significant quantity. Hence, there was no formation of charge compensating defects. This led to extremely low non-radiative channels and high quantum yield of 88%. Exploring Eu^{3+} luminescence in DFS offers a new, cheap, sustainable, and environmentally friendly designing strategy compared to other OPS based hosts to get rid of some problems in lanthanide doped phosphors

such as CCDs, cross contamination from $^5D_0 \rightarrow {}^7F_1$, and higher non-radiative channels for advanced optical, display, and lighting applications.

Credit author statement

Santosh K. Gupta- Conceptualization, Data curation, Formal analysis, Visualization, Writing – review & editing, Jose P Zuniga- Data curation, Methodology, Investigation, M.A.P. Garcia- Data curation, Methodology, Investigation, Bhupendra B. Srivastava- Data curation, Methodology, Investigation, Y. Mao- Conceptualization, Supervision, Visualization, Writing – review & editing.

Declaration of competing interest

The authors declare that they have no known competing financial interests or personal relationships that could have appeared to influence the work reported in this paper.

Acknowledgements

Y.M. would like to thank the financial support by the National Science Foundation under CHE (award #1952803 and 1710160) and the IIT start-up funds. SKG thanks the United States-India Education Foundation (USIEF) and the Institute of International Education (IIE) for his Fulbright Nehru Postdoctoral Fellowship (Award#2268/FNPDR/2017).

References

[1] Y.N. Ahn, K. Do Kim, G. Anoop, G.S. Kim, J.S. Yoo, Design of highly efficient phosphor-converted white light-emitting diodes with color rendering indices ($R_1 - R_{15}$) $\geq$ 95 for artificial lighting, Sci. Rep. 9 (2019) 1–10.

[2] Y. Li, Z. Qiu, J. Zhang, X. Ji, X. Zhang, S. Liao, W. Zhou, L. Yu, S. Lian, Highly efficient and thermally stable single-activator white-emitting phosphor $K_2Ca(PO_4)F:Eu^{2+}$ for white light-emitting diodes, J. Mater. Chem. C 7 (2019) 8982–8991.

[3] E. Song, X. Jiang, Y. Zhou, Z. Lin, S. Ye, Z. Xia, Q. Zhang, Heavy Mn^{2+} doped $MgAl_2O_4$ phosphor for high-efficient near-infrared light-emitting diode and the night-vision application, Adv. Optic. Mater. 7 (2019) 1901105.

[4] L. Sun, B. Devakumar, J. Liang, S. Wang, Q. Sun, X. Huang, A broadband cyan-emitting $Ca_2LuZr_2(AlO_4)_3:Ce^{3+}$ garnet phosphor for near-ultraviolet-pumped warm-white light-emitting diodes with an improved color rendering index, J. Mater. Chem. C 8 (2020) 1095–1103.

[5] S.K. Gupta, R. Kadam, P. Pujari, Lanthanide spectroscopy in probing structure-property correlation in multi-site photoluminescent phosphors, Coord. Chem. Rev. 420 (2020) 213405.

[6] S.K. Gupta, K. Sudarshan, B. Modak, A.K. Yadav, P. Modak, S.N. Jha, D. Bhattacharyya, Achieving bright blue and red luminescence in Ca_2SnO_4 through defect and doping manipulation, J. Phys. Chem. C 124 (2020) 16090–16101.

[7] R. Mani, S.K. Gupta, P.S. Ghosh, H. Jiang, Yellow emission from low coordination site of $Sr_2SiO_4:Eu^{2+},Ce^{3+}$: influence of lanthanide dopants on the electron density and crystallinity in crystal site engineering approach, Chem. Eur J. 24 (2018) 16149–16159.

[8] R. Devi, K. Singh, S. Vaidyanathan, Synergy in the energy transfer between ligands and Eu^{III} ions in molecular europium complexes: single-component white light-emitting luminogens, J. Mater. Chem. C 8 (2020) 8643–8653.

[9] M. Rajendran, S.K. Samal, S. Vaidyanathan, A novel self-activated (bluish-green) and Eu^{3+} doped (red) phosphors for warm white LEDs, J. Alloys Compd. 815 (2020) 152631.

[10] M. Rajendran, K. Singh, S. Vaidyanathan, A novel Sm^{3+}-activated $Li_3BaSrLn_3(MO_4)_8$ [Ln = La, Gd, and Y; M = Mo and W] deep red-emitting phosphors for plant cultivation and white LEDs, J. Info. Display (2020) 1–19.

[11] M. Rajendran, S. Vaidyanathan, Systematic investigation of Eu^{3+} activated $Na_2Ln_4(MoO_4)_7$ [Ln = La, Gd and Y] narrow band red emitting phosphors for hybrid white LEDs and plant growth, New J. Chem. 44 (2020) 14823–14836.

[12] M. Rajendran, S. Vaidyanathan, Zero-concentration quenching: a novel Eu^{3+} based red phosphor with non-layered crystal structure for white LEDs and $NaSrY(MoO_4)_3:Sm^{3+}$ based deep-red LEDs for plant growth, Dalton Trans. 49 (2020) 9239–9253.

[13] S.K. Gupta, M. Abdou, J.P. Zuniga, A.A. Puretzky, Y. Mao, Samarium-Activated $La_2Hf_2O_7$ nanoparticles as multifunctional phosphors, ACS Omega 4 (2019) 17956–17966.

[14] S.K. Gupta, K. Sudarshan, R.M. Kadam, Tunable white light emitting $Sr_2V_2O_7:Bi^{3+}$ phosphors: role of bismuth ion, Mater. Des. 130 (2017) 208–214.

[15] S.K. Gupta, J.P. Zuniga, M. Abdou, M.P. Thomas, M. De Alwis Goonatilleke, B. S. Guiton, Y. Mao, Lanthanide-doped lanthanum hafnate nanoparticles as multicolor phosphors for warm white lighting and scintillators, Chem. Eng. J. 379 (2020) 122314.

[16] H. Jia, Z. Wang, T. Yuan, F. Yuan, X. Li, Y. Li, Z.a. Tan, L. Fan, S. Yang, Electroluminescent warm white light-emitting diodes based on passivation enabled bright red bandgap emission carbon quantum dots, Adv. Sci. 6 (2019) 1900397.

[17] R. Sun, P. Lu, D. Zhou, W. Xu, N. Ding, H. Shao, Y. Zhang, D. Li, N. Wang, X. Zhuang, B. Dong, X. Bai, H. Song, Samarium-doped metal halide perovskite nanocrystals for single-component electroluminescent white light-emitting diodes, ACS Energy Lett. 5 (2020) 2131–2139.

[18] H. Wu, S. Wang, F. Cao, J. Zhou, Q. Wu, H. Wang, X. Li, L. Yin, X. Yang, Ultrastable inorganic perovskite nanocrystals coated with a thick long-chain polymer for efficient white light-emitting diodes, Chem. Mater. 31 (2019) 1936–1940.

[19] Z. Bai, H. Lin, J. Johnson, S.C.R. Gui, K. Imakita, R. Montazami, M. Fujii, N. Hashemi, The single-band red upconversion luminescence from morphology and size controllable Er^{3+}/Yb^{3+} doped MnF_2 nanostructures, J. Mater. Chem. C 2 (2014) 1736–1741.

[20] B.B. Srivastava, S.K. Gupta, Y. Mao, Single red emission from upconverting $ZnGa_2O_4$:Yb,Er nanoparticles co-doped by Cr^{3+}, J. Mater. Chem. C 8 (2020) 6370–6379.

[21] Z. Bai, H. Lin, K. Imakita, R. Montazami, M. Fujii, N. Hashemi, Synthesis of Er^{3+}/Yb^{3+} codoped $NaMnF_3$ nanocubes with single-band red upconversion luminescence, RSC Adv. 4 (2014) 61891–61897.

[22] H. Lin, D. Xu, A. Li, Z. Qiu, S. Yang, Y. Zhang, Enhanced red upconversion emission and its mechanism in Yb^{3+}–Er^{3+} codoped α-$NaLuF_4$ nanoparticles, New J. Chem. 41 (2017) 1193–1201.

[23] J. Wang, F. Wang, C. Wang, Z. Liu, X. Liu, Single-band upconversion emission in lanthanide-doped $KMnF_3$ nanocrystals, Angew. Chem. 123 (2011) 10553–10556.

[24] M.-Y. Xie, X.-N. Peng, X.-F. Fu, J.-J. Zhang, G.-L. Li, X.-F. Yu, Synthesis of Yb^{3+}/Er^{3+} co-doped MnF_2 nanocrystals with bright red up-converted fluorescence, Scripta Mater. 60 (2009) 190–193.

[25] S.K. Gupta, K. Sudarshan, P.S. Ghosh, A.P. Srivastava, S. Bevara, P.K. Pujari, R. M. Kadam, Role of various defects in the photoluminescence characteristics of nanocrystalline $Nd_2Zr_2O_7$: an investigation through spectroscopic and DFT calculations, J. Mater. Chem. C 4 (2016) 4988–5000.

[26] S.K. Gupta, K. Sudarshan, A.K. Yadav, R. Gupta, D. Bhattacharyya, S.N. Jha, R. M. Kadam, Deciphering the role of charge compensator in optical properties of $SrWO_4:Eu^{3+}$:A (A = Li+, Na+, K+): spectroscopic insight using photoluminescence, positron annihilation, and X-ray absorption, Inorg. Chem. 57 (2018) 821–832.

[27] K. Sudarshan, V. Tiwari, P. Utpalla, S.K. Gupta, Defect evolution in Eu^{3+}, Nb^{5+} doped and co-doped CeO_2: X-ray diffraction, positron annihilation lifetime and photoluminescence studies, Inorg. Chem. Front. 6 (2019) 2167–2177.

[28] P. Lecoq, M. Korzhik, New inorganic scintillation materials development for medical imaging, IEEE Trans. Nucl. Sci. 49 (2002) 1651–1654.

[29] Y.K. Liao, D.Y. Jiang, Y.P. Xu, J.L. Shi, Key Engineering Materials, in: Synthesis of Ultrafine $Lu_2Hf_2O_7$/Tb Phosphor by Solution Combustion Process, Trans Tech Publ, 2007, pp. 640–642.

[30] V. Trummel, S.K. Gupta, M. Pokhrel, D. Wall, Y. Mao, Investigating the impact of gamma radiation on structural and optical properties of Eu^{3+} doped rare-earth hafnate pyrochlore nanocrystals, J. Lumin. 207 (2019) 1–13.

[31] C. Woody, M. Furey, Fast Dense Low Cost Scintillator for Nuclear Physics, Brookhaven National Laboratory (BNL), Upton, NY (United States), 2009.

[32] M. Abdou, S.K. Gupta, J.P. Zuniga, Y. Mao, Insight into the effect of A-site cations on structural and optical properties of $RE_2Hf_2O_7$:U nanoparticles, J. Lumin. 210 (2019) 425–434.

[33] D. Nakauchi, G. Okada, N. Kawaguchi, T. Yanagida, Scintillation properties of $RE_2Hf_2O_7$ (RE = La, Gd, Lu) single crystals prepared by xenon arc floating zone furnace, Jpn. J. Appl. Phys. 57 (2018) 100307.

[34] J. Papan, D.J. Jovanović, K. Vuković, K. Smits, V. Đorđević, M. Dramićanin, Europium(III)-doped $A_2Hf_2O_7$ (A = Y, Gd, Lu) nanoparticles: influence of annealing temperature, europium(III) concentration and host cation on the luminescent properties, Opt. Mater. 61 (2016) 68–76.

[35] M. Pokhrel, K. Wahid, Y. Mao, Systematic studies on $RE_2Hf_2O_7$:5%Eu^{3+} (RE = Y, La, Pr, Gd, Er, and Lu) nanoparticles: effects of the A-site RE^{3+} cation and calcination on structure and photoluminescence, J. Phys. Chem. C 120 (2016) 14828–14839.

[36] S.K. Gupta, Y. Mao, Molten salt synthesis of metal oxide nanomaterials: status, opportunity, and challenge, Prog. Mater. Sci. (2020) 100734.

[37] J.P. Zuniga, M. Abdou, S.K. Gupta, Y. Mao, Molten-salt synthesis of complex metal oxide nanoparticles, JoVE (2018), e58482.

[38] S.K. Gupta, M.A.P. Garcia, Y. Mao, Excitation dependent site-specific luminescence and structure-optical property correlation of $Lu_2Sn_2O_7:Eu^{3+}$ nanoparticles, Opt. Mater. 109 (2020) 110357.

[39] S.K. Gupta, M.A.P. Garcia, J.P. Zuniga, Y. Mao, pH induced size tuning of $Gd_2Hf_2O_7:Eu^{3+}$ nanoparticles and its effect on their UV and X-ray excited luminescence, J. Lumin. 228 (2020) 117605.

[40] F.N. Sayed, V. Grover, K. Bhattacharyya, D. Jain, A. Arya, C. Pillai, A. Tyagi, $Sm_{2-x}Dy_xZr_2O_7$ pyrochlores: probing order-disorder dynamics and multifunctionality, Inorg. Chem. 50 (2011) 2354–2365.

[41] K.M. Turner, D.R. Rittman, R.A. Heymach, C.L. Tracy, M.L. Turner, A.F. Fuentes, W.L. Mao, R.C. Ewing, Pressure-induced structural modifications of rare-earth hafnate pyrochlore, J. Phys. Condens. Matter 29 (2017) 255401.

[42] S.K. Gupta, J.P. Zuniga, M. Abdou, P. Ghosh, Y. Mao, Optical properties of undoped, Eu^{3+} doped and Li^+ co-doped $Y_2Hf_2O_7$ nanoparticles and polymer nanocomposite films, Inorg. Chem. Front. 7 (2020) 505–518.

[43] S.K. Gupta, M. Abdou, P.S. Ghosh, J.P. Zuniga, Y. Mao, Thermally induced disorder–order phase transition of $Gd_2Hf_2O_7:Eu^{3+}$ nanoparticles and its implication on photo-and radioluminescence, ACS Omega 4 (2019) 2779–2791.

[44] M. Subramanian, G. Aravamudan, G.S. Rao, Oxide pyrochlores—a review, Prog. Solid Sate Chem. 15 (1983) 55–143.
[45] S.K. Gupta, M. Abdou, P.S. Ghosh, J.P. Zuniga, E. Manoharan, H. Kim, Y. Mao, On comparison of luminescence properties of $La_2Zr_2O_7$ and $La_2Hf_2O_7$ nanoparticles, J. Am. Ceram. Soc. 103 (2020) 235–248.
[46] S.K. Gupta, M. Abdou, J.P. Zuniga, P.S. Ghosh, E. Molina, B. Xu, M. Chipara, Y. Mao, Roles of oxygen vacancies and pH induced size changes on photo-and radioluminescence of undoped and Eu^{3+}-doped $La_2Zr_2O_7$ nanoparticles, J. Lumin. 209 (2019) 302–315.
[47] S.K. Gupta, P.S. Ghosh, C. Reghukumar, N. Pathak, R.M. Kadam, Experimental and theoretical approach to account for green luminescence from $Gd_2Zr_2O_7$ pyrochlore: exploring the site occupancy and origin of host-dopant energy transfer in $Gd_2Zr_2O_7$:Eu^{3+}, RSC Adv. 6 (2016) 44908–44920.
[48] S.K. Gupta, J.P. Zuniga, P.S. Ghosh, M. Abdou, Y. Mao, Correlating structure and luminescence properties of undoped and Eu^{3+}-doped $La_2Hf_2O_7$ nanoparticles prepared with different coprecipitating pH values through experimental and theoretical studies, Inorg. Chem. 57 (2018) 11815–11830.
[49] P.S. Dutta, A. Khanna, Eu^{3+}Activated molybdate and tungstate based red phosphors with charge transfer band in blue region, ECS J. Solid State Sci. Technol. 2 (2012) R3153–R3167.
[50] M. Keskar, S.K. Gupta, R. Phatak, S. Kannan, V. Natarajan, Optical properties of Eu^{3+} activated thorium molybdate and thorium tungstate: structure, local symmetry and photophysical properties, J. Photochem. Photobiol. Chem. 311 (2015) 59–67.
[51] A.H. Krumpel, P. Boutinaud, E. van der Kolk, P. Dorenbos, Charge transfer transitions in the transition metal oxides ABO_4:Ln^{3+} and APO_4:Ln^{3+} (A = La, Gd, Y, Lu, Sc; B = V, Nb, Ta; Ln = lanthanide), J. Lumin. 130 (2010) 1357–1365.
[52] A.K. Parchur, R.S. Ningthoujam, Behaviour of electric and magnetic dipole transitions of Eu^{3+}, $^5D_0 \rightarrow {}^7F_0$ and Eu–O charge transfer band in Li^+ co-doped YPO_4: Eu^{3+}, RSC Adv. 2 (2012) 10859–10868.
[53] A.M. Kaczmarek, D. Ndagsi, R. Van Deun, Dopant and excitation wavelength dependent color tunability in Dy^{3+}:YVO_4 and Dy^{3+}/Eu^{3+}:YVO_4 microparticles towards white light emission, Dalton Trans. 45 (2016) 16231–16239.
[54] C. Liu, F. Pan, Q. Peng, W. Zhou, R. Shi, L. Zhou, J. Zhang, J. Chen, H. Liang, Excitation wavelength dependent luminescence of $LuNbO_4$:Pr^{3+}—influences of intervalence charge transfer and host sensitization, J. Phys. Chem. C 120 (2016) 26044–26053.
[55] N. Jain, R. Paroha, R.K. Singh, S.K. Mishra, S.K. Chaurasiya, R.A. Singh, J. Singh, Synthesis and rational design of europium and lithium doped sodium zinc molybdate with red emission for optical imaging, Sci. Rep. 9 (2019) 2472.
[56] S.K. Gupta, M. Mohapatra, S.V. Godbole, V. Natarajan, On the unusual photoluminescence of Eu^{3+} in α-$Zn_2P_2O_7$: a time resolved emission spectrometric and Judd–Ofelt study, RSC Adv. 3 (2013) 20046–20053.
[57] B.G. Vats, S.K. Gupta, M. Keskar, R. Phatak, S. Mukherjee, S. Kannan, The effect of vanadium substitution on photoluminescent properties of $KSrLa(PO_4)_x(VO_4)_{2-x}$: Eu^{3+} phosphors, a new variant of phosphovanadates, New J. Chem. 40 (2016) 1799–1806.
[58] S.K. Gupta, C. Reghukumar, R.M. Kadam, Eu3+ local site analysis and emission characteristics of novel $Nd_2Zr_2O_7$:Eu phosphor: insight into the effect of europium concentration on its photoluminescence properties, RSC Adv. 6 (2016) 53614–53624.
[59] Y. Shi, D. Wu, Z. Wang, A new blue-light pumped red-emitting $NaYSnMoO_7$:Eu^{3+} pyrochlore phosphor for solid-state lighting, J. Mol. Struct. 1203 (2020) 127404.
[60] K. Vuković, S. Ćulubrk, M. Sekulić, M.D. Dramićanin, Analysis of luminescence of Eu^{3+} doped $Lu_2Ti_2O_7$ powders with Judd-Ofelt theory, J. Res. Phys. 38 (2015) 23–32.
[61] J.P. Zuniga, S.K. Gupta, M. Abdou, Y. Mao, Effect of molten salt synthesis processing duration on the photo- and radioluminescence of UV-, visible-, and X-ray-excitable $La_2Hf_2O_7$:Eu^{3+} nanoparticles, ACS Omega 3 (2018) 7757–7770.